Submitted to Nuclear Physics A

LBL-5042
Preprint

NUCLEAR RELAXATION PHENOMENA, DIFFUSION AND ORBITING IN THE REACTION $^{107,109}Ag + ^{84,86}Kr$ AT 7.2 MeV/NUCLEON

R. P. Schmitt, P. Russo, R. Babinet,
R. Jared, and L. G. Moretto

June 1976

Prepared for the U. S. Energy Research and
Development Administration under Contract W-7405-ENG-48

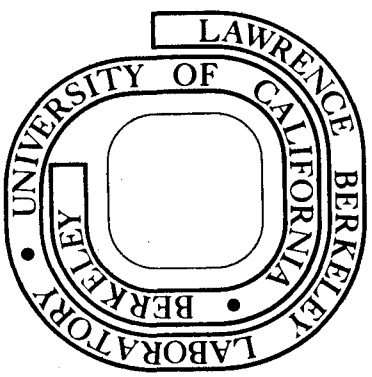

DISCLAIMER

NUCLEAR RELAXATION PHENOMENA, DIFFUSION AND ORBITING IN THE REACTION $^{107,109}Ag + ^{84,86}Kr$ at 7.2 MeV/NUCLEON

R. P. Schmitt, P. Russo, R. Babinet*,
R. Jared and L. G. Moretto†

Nuclear Science Division
Lawrence Berkeley Laboratory
University of California
Berkeley, California 94720

ABSTRACT

Charged particles produced from the interaction of a 7.2 MeV/nucleon Kr beam and a natural Ag target have been studied. Fragments up to Z = 50 have been identified by means of an ΔE,E telescope. Kinetic energy distributions, charge distributions and angular distributions have been measured for the individual atomic numbers. The kinetic energy distributions show two components: a high energy "quasi-elastic" component, and a low energy or "relaxed" component close to the Coulomb energy for touching spheres. The charge distribution for this system is very broad and appears to peak at symmetry rather than at the Z of the projectile. The angular distributions for the relaxed component increase monotonically with decreasing angle and are all forward peaked in excess of $1/\sin\theta$. These results are dramatically different from those obtained in Kr bombardments of heavier targets where rather narrow charge distributions and side peaked angular distributions have been observed. The behavior of the reaction Ag + Kr is strongly reminiscent of reactions induced by lighter projectiles. An interpretation of these data in terms of a diffusion process along the mass asymmetry coordinate is presented.

---

*Present address DphN/MF - CEN, Saclay, France.
†Sloan Fellow 1974 - 1976.

NUCLEAR REACTIONS $^{107,109}Ag(^{84,86}Kr,x)$,
E = 606, 620 MeV; measured
$\sigma(E,\theta,Z)$, $9 \leq Z \leq 50$.

Introduction

Reaction studies of the light fragments emitted in ^{14}N, ^{20}Ne and ^{40}Ar bombardments of various targets[1-6] have revealed the presence of a nearly thermalized or relaxed component at energies close to the Coulomb energy for touching spheres.

The fission-like kinetic energy distributions imply that substantial energy equilibration has been achieved in these systems. On the other hand, the shape of the observed charge distributions is strongly dependent on the entrance channel. Angular distributions for the relaxed component are forward peaked in excess of $1/\sin\theta$ for fragments in the vicinity of the projectile. The charge and angular distributions indicate a pronounced lack of equilibration with respect to the mass asymmetry degree of freedom. These observations effectively ruled out the possibility of a compound nucleus mechanism, and led to an interpretation in terms of an intermediate complex, consisting of touching fragments, evolving along the mass asymmetry degree of freedom via a diffusion process[7-9]. Quantitative calculations are in excellent agreement with the experimental results.

Relaxation and diffusion phenomena have also been observed in very heavy systems like Kr + Bi[10,11]. However, the characteristics of the so-called quasi-fission process seem substantially different from those considered above: the mass distributions are peaked about the projectile and the gross angular distribution (all products taken simultaneously) is side peaked. More detailed studies[12] have shown that these features in no way contradict the hypothesis of a diffusion process; in fact,

the same model, so successful when applied to lighter systems, is capable of reproducing the data,[13] and thus presents a unified approach to the interpretation of heavy ion reactions.

Most of the experiments done with projectiles heavier than ^{40}Ar have involved heavy targets and, therefore, strong Coulomb fields. The currently available energy range of such beams has confined such studies to energies about 1.5 times the interaction barrier. On the other hand, many of the detailed studies of ^{40}Ar induced reactions have been carried out at energies greater than twice the interaction barrier. It has been shown that the differences in the charge and angular distributions observed in Ar reactions and Kr reactions reflect the difference in the ratio E/B (i.e. $E_{c.m.}/B_{Coulomb}$), rather than a difference in the total mass of the system.[14] The current system, Ag + Kr, gives 1.9 for E/B, and, therefore, may aid in establishing the usefulness of the parameter E/B in predicting the character of the charge and angular distributions.

Another attractive feature of this system is the fact that the initial configuration is close to symmetry, where the potential energy vs. mass/charge asymmetry is rather flat. Thus the predicted charge distributions should be in striking contrast with systems like Au + ^{40}Ar[6], where the potential energy changes rapidly as a function of mass asymmetry.

Finally, but of paramount importance, the characteristics of such a system should help in extracting coefficients involved in nuclear transport phenomena.

Experimental Techniques

The Kr beams used in this experiment had an energy of 7.2 MeV/A and were produced by the Berkeley SuperHILAC. The initial measurements were

made with a ^{84}Kr beam. Because naturally occurring Kr was used in the source (57% ^{84}Kr), the beam intensity was less than that obtained when isotopically enriched ^{86}Kr was used. As a result, subsequent measurements were made with a ^{86}Kr beam at the same energy per nucleon. It can be argued that the system produced in ^{86}Kr bombardment is different in both mass and excitation energy; however, it should be noted that two neutrons represent a rather small fraction of the total system and that the 4 MeV difference in E_{cm} for the two systems is of the same order as the uncertainty in the beam energy.

The beam was collimated on target to a diameter of about 3 mm by means of a system of concentric rings of low Z material, either carbon or boron nitride. The natural silver targets were self-supporting with typical thicknesses of 500 $\mu g/cm^2$. After penetrating the target, the beam was collected in a Faraday cup. Except for very forward angles, where elastic scattering prohibited high beam currents, the beam intensity ranged from 30 to 150 nA electrical with an average of about 50 nA.

Reaction products were detected with two or four $\Delta E,E$ telescopes[15], consisting of gas ionization ΔE detectors and solid state E detectors, mounted on two movable arms. Pure methane was used in the detectors at gas pressures ranging from 8 to 40 cm of Hg. The gas pressure was controlled by a Cartesian-manostat. For pressures less than 10 cm of Hg, Formvar entrance windows approximately 50 $\mu g/cm^2$ were used on the telescopes. For higher pressures, 280 $\mu g/cm^2$ polycarbonate (Kimfoil) windows were used. In order to prevent poisoning of the gas, high flow rates were maintained.

The entrance windows to the telescopes were mounted from 7 to 15 cm from the center of the chamber. This corresponds to an angular acceptance of 2.5° in the reaction plane for the closest position. The absolute efficiencies of the telescopes were measured with a ^{241}Am α-source of known activity and the asymmetry of the chamber was determined by taking elastic scattering data at both positive and negative angles.

Signals from the telescopes were fed to linear and logic circuitry described elsewhere[5]. Coincident ΔE and E signals were digitized by an analog multiplexer-ADC system. The digitized information including marker bits to identify the origin of the event was fed to a PDP-15 computer via a CAMAC system. For the backward angles, the dead times were less than 10%. In the angular regions where elastic scattering was present, the dead times were kept below about 40% by limiting the beam current. To further insure that the measurements were not distorted by high counting rates, a pulser signal of fixed amplitude was run through the system both between and during beam bursts.

Monitoring of the experiment was accomplished on-line with a two dimensional display of E and ΔE arrays and off-line by printing out expanded arrays with the aid of a PDP-9 computer.

Data Reduction

The off-line analysis of the data was performed on a PDP-9 computer. Initially, the two-dimensional data was printed as a ΔE-E map of dimensionality 960 × 100. The charged particles produced in the reaction appeared as ridges on this map. In the initial experiments with ^{84}Kr, individual charges were visible up to $Z \cong 40$. Technological improvements

in latter experiments performed with ^{86}Kr extended the resolution to $Z \cong 50$. The maximum resolved Z obtained in these experiments is dependent on fragment energy and therefore angle. As a result more charges were resolved at forward angles where the energy is highest.

At forward angles the actual atomic numbers of the fragments were identified by the presence of the elastically scattered projectile. At more backward angles the Z calibration was obtained through a comparison with forward angles, and by the presence of a low energy tail for Z = 36 presumably due to secondary scattering and/or slit scattering. Boundaries for the Z ridges were determined either by visual inspection or by an automatic procedure described elsewhere[16]. Kinetic energy spectra were then produced by summing the regions of the individual Z's.

Energy calibrations were obtained from short runs of elastic scattering with and without gas in the ΔE detector. These measurements agreed reasonably well with those obtained with a precision Hg pulser system and are probably good to about 3%.

The resulting laboratory kinetic energy distributions were corrected for the effect of the window and target using polynomial fits to the Northcliff-Schilling range energy tables. In addition, a correction for the pulse height defect was made using the relation[17]:

$$\Delta\varepsilon = \frac{6.\varepsilon}{\varepsilon + 8} + \frac{18.}{1 + 525.\varepsilon^{-1.407}} \quad ,$$

where $\Delta\varepsilon$ is the pulse-height defect of the ion in silicon for energy ε.

All energies are L.S.S. units[18] defined by:

$$\Delta\varepsilon = k(Z,A)\Delta E$$

$$\varepsilon = k(Z,A)E \quad ;$$

where $\Delta\varepsilon$ and ε are in MeV and:

$$k(Z,A) = \frac{6.53 \times 10^4}{Z(Z^{2/3} + 5.81)^{1/2}\,(A + 28.1)}$$

where Z and A are the charge and mass of the particle.

The corrected laboratory spectra were then transformed to the center of mass assuming binary division and charge-to-mass equilibration of the complex at fixed mass asymmetry[9]. That is, for a fixed mass asymmetry of the complex, the resulting charge is that which minimizes the liquid drop potential energy of the system.

The transformation of the laboratory kinetic energy distributions is easily accomplished in view of the fact that:

$$\left.\frac{\partial^2\sigma}{\partial\Omega'\partial\varepsilon}\right|_{cm} = \left.\frac{\partial^2\sigma}{\partial\Omega\partial E}\right|_{lab} \times \frac{\sin\theta}{\sin\psi} \quad ,$$

where Ω, E, θ and Ω', ε, ψ are the respective solid angles, energy and angle in the lab and center of mass systems.

The kinetic energy distributions were then edited interactively to correct for the various experimental effects which might distort the data, like energy cutoffs and secondary scattering or slit scattering for Z = 36. The latter effect is quite significant for forward angles for Z's adjacent to the projectile, and it can account for as much as

50% of the relaxed peak for Z = 36. Another problem arises from the elastic scattering contaminating the high energy part of the spectra for Z = 35,37. At all angles but the grazing, the "elastic spillover" is easily identified in the neighboring Z's and has been removed. In addition, the elastic has been removed from the spectra for Z = 36 whenever it appeared as a distinct component. No attempt was made to analyze the elastic scattering data as the angular acceptance (as large as 2.5°) made it unfeasible to do so. The following quantities were calculated from the spectra:

i) the total cross section

$$\left(\frac{d\sigma}{d\Omega}\right)_{c.m.} = \int \left(\frac{\partial^2\sigma}{\partial\Omega\partial E}\right)_{c.m.} dE_{c.m.} \quad ;$$

ii) the mean kinetic energy

$$E_{c.m.} = \left(\frac{d\sigma}{d\Omega}\right)^{-1}_{c.m.} \int E_{c.m.} \left(\frac{\partial^2\sigma}{\partial\Omega\partial E}\right)_{c.m.} dE_{c.m.} \quad ;$$

iii) and the mean angle

$$\theta_{c.m.} = \left(\frac{d\sigma}{d\Omega}\right)^{-1}_{c.m.} \int \theta_{c.m.} \left(\frac{\partial^2\sigma}{\partial\Omega\partial E}\right)_{c.m.} dE_{c.m.} \quad .$$

The lab cross sections so obtained are generally reproducible to within about 10%, reflecting the relative errors in the measurements. The absolute errors on the cross sections are probably not greater than about 25%. Some general kinematical features of this system are given in Table I.

Results and Discussion

1. Kinetic Energy Distributions

The kinetic energy distributions of the reaction products reveal the existence of two components (in addition to elastic scattering): a quasi-elastic peak, at near elastic energies; and a deep-inelastic, or relaxed, component at substantially lower energies. The existence of these two components has already been confirmed with lighter projectiles like ^{14}N, ^{20}Ne and ^{40}Ar.[1-6] This is somewhat atypical of Kr reactions with heavier target where the quasi-elastic and relaxed components often lose their separate identities[19]. Representative spectra are given in Fig. 1(a), (b).

This figure shows that the quasi-elastic component is restricted to forward angles and to atomic numbers close to that of the projectile. As was mentioned above, the elastically scattered projectile tends to contaminate the spectra for adjacent atomic numbers. The removal of this component is somewhat uncertain for 19.5° because the quasi-elastic peak attains its maximum energy at this angle, resulting in some overlap.

For angles forward of the grazing, the distinction between quasi-elastic and deep-inelastic diminishes, and very broad distributions are observed for elements around Kr. Sufficiently behind the grazing angle, a single, fully relaxed peak is visible. In this angular range the spectra are approximately Gaussian. The width of this peak is essentially independent of angle implying a constant degree of energy relaxation over a broad angular range.

The dependence of the shapes of kinetic energy distributions with angle is very similar to that observed in Ar induced reactions. Just

such a pattern, observed in the reaction Th + Ar, lead Wilczynski to an interpretation in terms of orbiting[20]. For rather high impact parameters only small amounts of matter and/or energy are transferred. Fragments produced in these collisions follow near Coulomb trajectories and account for the quasi-elastic component near the grazing angle. As the impact parameter is decreased, more energy and mass are transferred and the fragments are deflected towards smaller angles. At still lower impact parameters, "sticking" of the fragments occurs, and the complex may rotate past 0° to negative angles in the reaction plane. At backward angles, only the damped long range "orbiting" component is observed. The overlap of the positive and negative angle contributions leads to broad energy distributions for forward angles.

The mean center of mass kinetic energy and FWHM of the relaxed peak averaged over a large angular range (24° to 70° in the lab) is shown in Fig. 2 for the various fragments. Two trends are evident in this figure: the constancy of the mean c.m. energy and FWHM as a function of angle and the proximity of the mean energies to that arising from the repulsion of two touching spherical fragments. Similar trends have been observed in reactions induced by lighter projectiles like ^{40}Ar, making it reasonable to assume that the mechanism involved in the reaction Ag + Kr is similar.

The energies given in Fig. 2 have not been corrected for particle emission. Reasonable estimates based on the available excitation energies and the assumption of neutron emission indicate that the initial mean kinetic energies for the relaxed peak are at worst about 12% higher than the plotted values. The complication of particle

evaporation and the problem of an unknown ℓ-distribution make it difficult to extract detailed information regarding the shape of the fragments at the moment of decay. However, it seems from the data that even corrected for particle evaporation, the observed energies are lower than those expected for spherical fragments, implying some deformation in the complex at scission.

The large widths of the relaxed energy spectra can be understood in terms of a model employing shape polarization of the fragments.[24] Semi-quantitative agreement has been obtained for the case $^{107,109}Ag + {}^{14}N$.[4] Again particle emission and an uncertain ℓ-distribution complicate the matter and make quantitative fits impractical.

The overall behavior of the kinetic energy spectra with angle for this reaction is very similar to that obtained with lighter ions, and provides strong evidence for orbiting. Further discussion of the orbiting in the reaction Ag + Kr will be given in the last section.

Laboratory Charge Distributions

Laboratory cross sections integrated over energy for various atomic numbers and for several angles are given in Fig. 3(a),(b). For angles behind the grazing, only the deep-inelastic or relaxed component contributes to the cross section. The observed charge distributions for these angles are very broad and the cross section increases with increasing Z. At more forward angles the quasi-elastic component becomes dominant for Z close to Z = 36, and a good deal of the cross section is concentrated in this region. The yield for the quasi-elastic

component is distributed more or less symmetrically about Z = 36. This is not surprising since the target and projectile are similar in mass so that stripping and pickup are similar processes. When the quasi-elastic component is removed, the distributions look very similar to those obtained at backward angles and peak near symmetry (Z = 41.5).

The charge distributions for the relaxed component of the reaction Ag + Kr are very different from those obtained with Kr projectiles and heavy targets[10-12] (in these cases the "quasi-fission" yield peaks near the projectile Z), and resemble the broad distributions observed with lighter projectiles like ^{40}Ar. These observations support the contention that it is the ratio E/B that determines the shape of the mass distribution and not the total mass of the system[14].

The charge and angular distributions produced in ^{14}N, ^{20}Ne and ^{40}Ar bombardments have been interpreted in terms of a diffusion model in which target and projectile combine to form an intermediate complex consisting of two touching fragments which evolves along the mass/charge asymmetry mode via a diffusion mechanism. Predictions of this model for Ag + 288 MeV Ar are in very good agreement with experimental results[8]. Recently, the diffusion model has been successfully extended to very heavy systems like Au + Kr providing strong evidence that the deep-inelastic and quasi-fission processes are the same[13].

The liquid drop potential energy as a function of charge asymmetry (ridge-line potential) is given in Fig. 4 for several ℓ-waves. The calculation assumes that the complex consists of touching spherical fragments. For all ℓ-wave the injection point (i.e., entrance channel mass asymmetry) is close to the potential minimum, and as a result,

the diffusion process causes rapid spreading in mass asymmetry. Results of diffusion calculations are given in Fig. 5. The pattern of the experimental charge distributions is qualitatively reproduced.

These charge distributions alone do not tell us if equilibrium has been achieved with respect to the mass asymmetry mode. One expects that the equilibrium Z-distribution, Y(Z), should be given by

$$Y(Z) = K(Z,\ell) \exp(-V_Z/T) \quad ,$$

where V_2, T and ℓ are the potential energy, temperature and angular momentum, and K is a slowly varying function of its independent variables. Detailed comparisons of a variety of target-projectile combinations indicate that the relaxation of this mode is slow when compared with that of other modes like the dissipation of energy and equilibration of the N/Z ratio.[13,14,22]

Charge Distributions For Different Kinetic Energy Windows

Since the distinction between the quasi-elastic and relaxed components is, in some cases, not well defined, we have generated Z-distributions for various energy windows (see Fig. 6). These distributions have been obtained by integrating the center of mass kinetic energy spectra between $E_{c.m.}$ vs Z lines parallel to the experimental mean $E_{c.m.}$ vs Z line (see Fig. 2) obtained at backward angles, and integrating over center of mass angles. This procedure thus defines energy lines relative to the relaxed energy line.[14]

For high kinetic energies, the distributions are fairly narrow and are peaked at the projectile Z. As one moves towards lower kinetic

energies, the centroids move towards higher Z and become broader. The shape of the distributions does not change over the last few lines. This is expected since the energy spread in this region is due to shape polarization of the fragments and is not a continuation of the energy damping process.

The total cross section integrated over energy and angle as a function of Z is given in Fig. 7. The peaking around Z = 36 is due to the quasi-elastic component. The total cross section summed over Z is 1.7b. This number is considerably smaller than the calculated value 2.6b. However, since the angular distributions are forward peaked, a large fraction of the cross section may be outside the range of the experimental measurements.

Angular Distributions

The center of mass angular distributions are given in Fig. 8. In the cases where a decomposition of the quasi-elastic and relaxed components was feasible, both the relaxed and total are given. The angular distributions $\frac{d\sigma}{d\Omega}$ vs θ are all forward peaked in excess of $1/\sin\theta$ (with the exception of Z = 9,10). To make this more readily visible we have plotted $\frac{d\sigma}{d\theta}$ rather than $\frac{d\sigma}{d\Omega}$.

It should be noted, that until this point, no experimental evidence has been given to rule out the possibility of a compound nucleus mechanism for the relaxed component of the reaction Ag + Kr. If the mechanism were fission of a compound nucleus, the angular distributions would be $1/\sin\theta$ in $\frac{d\sigma}{d\Omega}$ (or flat in $\frac{d\sigma}{d\theta}$). It is now evident that, while some compound nucleus fission may be present, such a mechanism cannot be the dominant one.

The forward peaking in excess of $1/\sin\theta$ implies that the lifetime of the intermediate complex is comparable to the rotational period (about 6×10^{-21} sec for the r.m.s. angular momentum assuming that the complex consists of spherical fragments in contact and rotating rigidly). The excess forward peaking is strongest in the vicinity of the projectile. As one moves down in Z, the forward peaking decreases gradually until about Z = 17, where it tends to increase again, and then decreases again. This behavior for the very low Z's is not easily explained, and may be an experimental effect due to secondary reactions with a low Z material like Al.

This pattern of angular distributions can be qualitatively accounted for within the framework of the diffusion model. One expects to see the greatest forward peaking for the shortest lifetimes. At the same time, short lifetimes imply small mass transfers. Hence, one observes the greatest forward peaking in the vicinity of the projectile. Atomic numbers far from the projectile are populated on a much longer time scale, so the complex has, on the average, rotated through much larger angles. As a result, the angular distributions are less forward peaked.

While patterns similar to the present one have been observed in the angular distributions of N, Ne and Ar induced reactions[1-6], the distributions for the reaction Ag + Kr are in striking contrast to those obtained in Kr bombardments of heavy targets like Bi and Au[10-12]. In the latter cases, the gross product (i.e. the sum of all masses) angular distributions are side peaked. Such contrasting behavior can be attributed to differences in the ratio τ_{life}/τ_{rot}, where τ_{life} and τ_{rot} represent the average lifetime and the average rotational period

of the complex. For small values of this ratio, the complex does not live long enough to reach 0°, and the fragments are emitted on the side of impact. For slightly larger values, the complex decays at angles near 0° producing angular distributions that are forward peaked. As the value of this ratio increases further, the complex rotates to larger negative angles before decaying, resulting in decreased forward peaking and enhanced yields in the backward hemisphere. In the limit of large τ_{life}/τ_{rot}, the complex may undergo one or more complete revolutions, and the angular distributions tend to the $1/\sin\theta$ behavior expected for the decay of a compound nucleus with large angular momentum.

There is rather extensive experimental evidence to support this picture. The reactions Ag + Ne^{5} and Au + Kr^{12} are good examples. In the former case, there is a continuous evolution from enhanced forward peaking near the projectile to $1/\sin\theta$ behavior 4 or 5 Z units above Ne. In the latter case, a transition occurs from side peaking to forward peaking as more mass is transferred. The variation in the angular distributions can, in both cases, be attributed to the effective time delay associated with increased mass transfer. That is, the time delay in populating configurations very different from the entrance channel effectively increases the ratio τ_{life}/τ_{rot}.

The angular distributions for the Ag + Kr are intermediate to those of the two systems discussed above: excluding the quasi-elastic, there is no side peaking; however, the $1/\sin\theta$ limit is not attained even after the transfer of over 20 charge units.

The value of τ_{rot} can be estimated with simple models like touching spheres rotating rigidly. However, the lifetime is more difficult to calculate. Values of the lifetime for the reactions Ag + 288 MeV Ar and Au + 620 MeV Kr have been obtained by fitting the angular distributions with the diffusion model of Moretto and Sventek;[8,13] but, in general, the ratio τ_{life}/τ_{rot} is not readily available for an arbitrary system.

There is empirical evidence that the ratio E/B is useful in predicting the character of charge and angular distributions, implying that the lifetime of the intermediate complex is dynamically controlled. For values of E/B $\leq$ 1.6, side peaking is observed. For larger E/B values, the angular distributions are forward peaked. The ratio is about 1.9 for Ag + 620 MeV Kr, and, in agreement with energing systematics, the angular distributions are forward peaked. A more detailed discussion of the E/B effect and its connection with the ratio τ_{life}/τ_{rot} is given in Ref. 14.

Wilczynski Diagrams

As a final presentation of the data we have constructed Wilczynski diagrams[17] for the individual atomic numbers. Representative examples are shown in Fig. 9. In constructing these diagrams the center of mass kinetic energy distributions have been converted to $\partial^2\sigma/\partial E_T \partial\theta$ by multiplying by sin θ and converting to total center of mass energy assuming binary division. Intermediate angles have been estimated by linearly interpolating between adjacent spectra. Contours of constant cross section have then been drawn with the aid of a CDC-7600 computer.

On such a plot, a $1/\sin\theta$ angular distribution will yield a series of horizontal parallel contours. For Z's very far from the projectile, such behavior is approached but never fully attained. For small center of mass angles, the contours indicate that the distributions are forward peaked in excess of $1/\sin\theta$.

For all Z's the relaxed component appears as a low energy ridge approximately parallel to the θ-axis. For atomic numbers close to that of the projectile, there is a second ridge extending for the quasi-elastic peak towards lower energies at smaller angles. These patterns are strong evidence for orbiting in the reaction Ag + Kr^{20}.

In this picture, the high energy ridge is composed of decay products from the short-lived intermediate complex formed at high impact parameters. Because of the short times involved, the kinetic energy is only partially damped and the complex has not undergone large angular deflections past 0°.

The low energy branch results from the decay of the complex formed smaller impact parameters where longer lifetimes have allowed more complete relaxation and rotations past 0° to large negative angles. There is some doubt as to the origin of the yield at very backward angles. It could be produced when the complex orbits past 0° and decays at backward angles. On the other hand, it may be associated with low ℓ-waves. In the latter case, a large overlap of nuclear matter may lead to a long-lived intermediate essentially equilibrated in energy. The low angular velocities involved would tend to inhibit large rotations so that the complex would decay at backward angles. On the

basis of results obtained in the reaction Au+Kr[12] and compound nucleus studies with heavy projectiles[21], the latter explanation is attractive. However, the first possibility cannot really be excluded on the basis of the data obtained in the present study.

It is interesting to note that the orbiting characteristics become less pronounced for larger mass transfers. For atomic numbers far from the projectile, only the low energy branch is visible. This is consistent with diffusive evolution along the mass/charge asymmetry mode provided that the energy relaxation occurs more rapidly. This is particularly apparent in experiments in which both the mass and charge of deep-inelastic reaction products have been measured simultaneously[22,23].

Summary and Conclusions

Nuclear relaxation phenomena are clearly visible in the reaction Ag + Kr. Most apparent are the relaxation of energy as seen in the kinetic energy spectra for Z's close to that of the projectile and relaxation of the mass/charge asymmetry mode, as reflected in the charge and angular distributions. The relaxation along the mass asymmetry mode seems to be slower than the relaxation of kinetic energy and appears to be diffusive in nature. The charge and angular distributions have been interpreted within the framework of the diffusion model of Moretto and Sventek and provide evidence for such a unified approach in the interpretation of heavy ion reaction phenomena. Finally, the experimental data show that nuclear orbiting is well developed in the reaction Ag + Kr.

References

1. L. G. Moretto, D. Heuneman, R. C. Jared, R. C. Gatti and S. G. Thompson, Physics and Chemistry of Fission, 1973. (Intern. Atomic Energy Agency, Vienna, 1974), Vol. II, p. 351.

2. A. G. Artukh, G. F. Gridnev, V. L. Mikheev, V. V. Volkov and J. Wilczynski, Nucl. Phys. A215 (1973) 91.

3. L. G. Moretto, S. K. Kataria, R. C. Jared, R. Schmitt and S. G. Thompson, Nucl. Phys. A255 (1975) 491.

4. J. Galin, L. G. Moretto, R. Babinet, R. Schmitt, R. Jared and S. G. Thompson, Nucl. Phys. A255 (1975) 472.

5. R. Babinet, L. G. Moretto, J. Galin, R. Jared, J. Moulton and S. G. Thompson, Nucl. Phys. A258 (1976) 172.

6. L. G. Moretto, J. Galin, R. Babinet, Z. Fraenkel, R. Schmitt, R. Jared and S. G. Thompson, Nucl. Phys. A259 (1976) 173.

7. L. G. Moretto, R. P. Babinet, J. Galin and S. G. Thompson, Phys. Lett. 58B (1975) 31.

8. L. G. Moretto and J. S. Sventek, Phys. Lett. 58B (1975) 26.

9. B. Gatty, D. Guerreau, M. Lefort, J. Pouthas, X. Tarrago, J. Galin, B. Cauvin, J. Girard and H. Nifenecker, Z. Physik A273 (1975) 65.

10. F. Hanappe, M. Lefort, C. Ngô, J. Peter and B. Tamain, Phys. Rev. Lett. 32 (1974) 738.

11. K. L. Wolf, J. P. Unik, J. R. Huizenga, J. Birkelund, H. Freiesleben and V. E. Viola, Phys. Rev. Lett. 33 (1974) 1105.

12. L. G. Moretto, B. Cauvin, P. Glässel, R. Jared, P. Russo, J. Sventek and G. Wozniak, Phys. Rev. Lett. 36 (1976) 1069.

13. J. S. Sventek and L. G. Moretto, Lawrence Berkeley Laboratory Report LBL-5012, submitted to Phys. Lett.; L. G. Moretto and J. S. Sventek, Proc. of the Symp. on Macroscopic Features of Heavy Ion Collisions, Argonne, Ill., 1976 (LBL-5006).

14. L. G. Moretto and R. Schmitt, European Conference on Nuclear Physics with Heavy Ions, Caen, 1976 (LBL-5057).

15. M. M. Fowler and R. C. Jared, Nucl. Instr. and Meth. 124 (1975) 341.

16. P. Glässel, R. Jared and L. G. Moretto, to be published.

17. S. B. Kaufman, E. P. Steinberg, B. D. Wilkins, J. Unik, A. J. Groski and M. J. Cluss, Nucl. Instr. Meth. 115 (1974) 47.

18. J. Lindhard, M. Scharff and H. E. Schiott, Mat. Fys. Medd. Dan. Vicl. Selsk 33, No. 14 (1963) 1.

19. P. Russo, R. P. Schmitt, G. J. Wozniak, R. Jared, P. Glässel, B. Cauvin and L. G. Moretto, to be published.

20. J. Wilczynski, Phys. Lett. 47B (1973) 484.

21. C. Cabot, H. Gauvin, Y. LeBeyec and M. Lefort, J. de Physique L36 (1975) 289.

22. J. Galin, European Conference on Nuclear Physics with Heavy Ions, Caen, 1976.

23. J. Galin, B. Gatty, D. Guerreau, M. Lefort and X. Tarrago, Orsay preprint.

Table 1. Characteristics of the reaction $^{108}Ag + ^{86}Kr$ at 620 MeV bombarding energy.

$E_{c.m.}$ (MeV)	345.
$E^*_{c.n.}$ (MeV)	191.
$T_{c.n.}$ (MeV)	2.8
L_{max} ($\hbar$)	255.
σ_r (b)	2.57
$\theta^{crit}_{c.m.}$ (deg)	43.
$B_{Coulomb}$ (MeV)	184.
τ_{rot} (sec)	6.5×10^{-21}

An R_o of 1.2249 fm was used in calculating the nuclear radii. In addition, 2.0 fm was added to the sum of the radii in the calculations. The temperature was obtained from $T_{c.n.} = \sqrt{E^*_{c.n.}/a}$ assuming $a = A/8$ and $\ell = 0\hbar$. The rotational period τ_{rot} is given for the entrance channel mass asymmetry and assumes $\ell = \ell_{r.m.s.}$ and spherical fragments.

Figure Captions

Fig. 1 (a),(b) Center of mass kinetic energy distributions for various atomic numbers at four lab angles. For purpose of comparison with other Z's, the elastic component has been extracted from Z = 36 at 9.5° and 19.5°.

Fig. 2 Mean center of mass energies and FWHM's for the relaxed peak averaged over a broad angular range (24° to 70° in the lab) as a function of fragment Z. The error bars correspond to one standard deviation from the mean.

Fig. 3 (a) Laboratory charge distributions for $^{107,108}Ag$ + 620 MeV ^{86}Kr at various lab angles. The cross section for the relaxed component is shown when it was possible to make a distinction between it and the quasi-elastic.

(b) Same as (a) for $^{107,109}Ag$ + 606 Mev ^{84}Kr. At these more backward angles, the kinetic energy spectra are essentially all relaxed.

Fig. 4 Ridge-line potential energies for ^{108}Ag + ^{86}Kr for various angular momenta. The energies are plotted relative to the entrance channel.

Fig. 5 Diffusion model calculations of contours of constant population in the plane defined by the charge asymmetry coordinate and the time for the same ℓ-waves given in Fig. 4.

Fig. 6 Charge distributions (integrated over angle from θ_{lab} = 9.5° to 55°) for various kinetic energy bins. The bins are 20 MeV wide. The bin number multiplied by 20 gives the upper energy limit of the bin in MeV for Z = 36.

Fig. 7 Total cross section for all non-elastic energies integrated over angle from θ_{lab} = 9.5° to 55° as a function of Z. The dashed curve at Z = 36 reflects the uncertainty in distinguishing elastic and non-elastic events.

Fig. 8 Center of mass angular distributions for 32 atomic numbers. The quantity $d\sigma/d\theta$ is plotted. Both the relaxed and total contributions are given when the relaxed component appeared as a distinct component. The number in parenthesis is the common log of the multiplication factor.

Fig. 9 Contours of constant center of mass cross section $\partial^2\sigma/\partial\theta\partial E$ in the plane defined by center of mass angle θ and total center of mass kinetic energy E. The spacing as given by $\partial^2\sigma/\partial\theta\partial E = 2^3, 2^4, \ldots$ μb/rad-MeV.

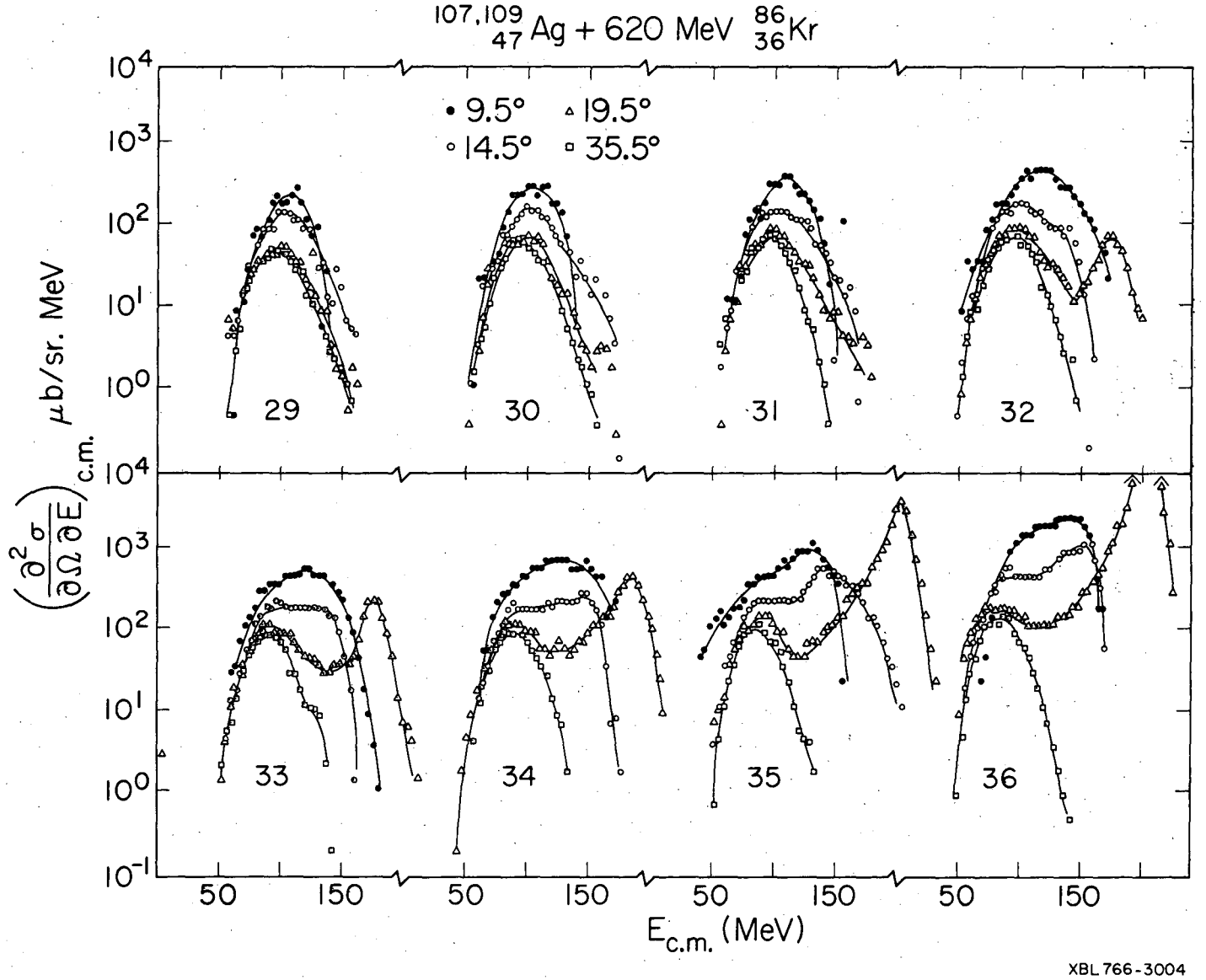
107,109 47 Ag + 620 MeV 86 36 Kr
• 9.5° △ 19.5°
○ 14.5° □ 35.5°
29
30
31
32
33
34
35
36
μb/sr. MeV
(∂²σ/∂Ω∂E)c.m.
Ec.m. (MeV)
XBL 766-3004

Fig. 1a

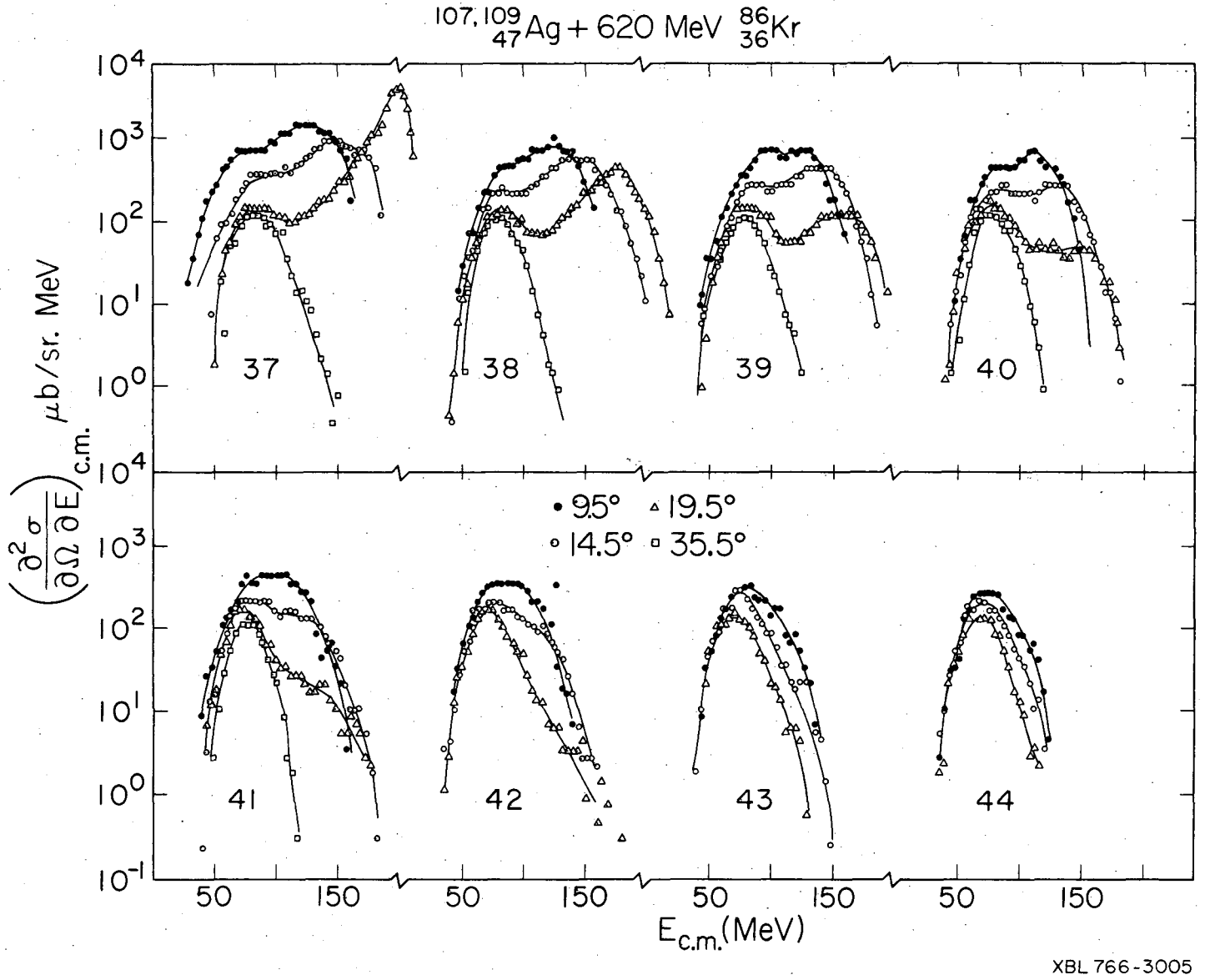

Fig. 1b

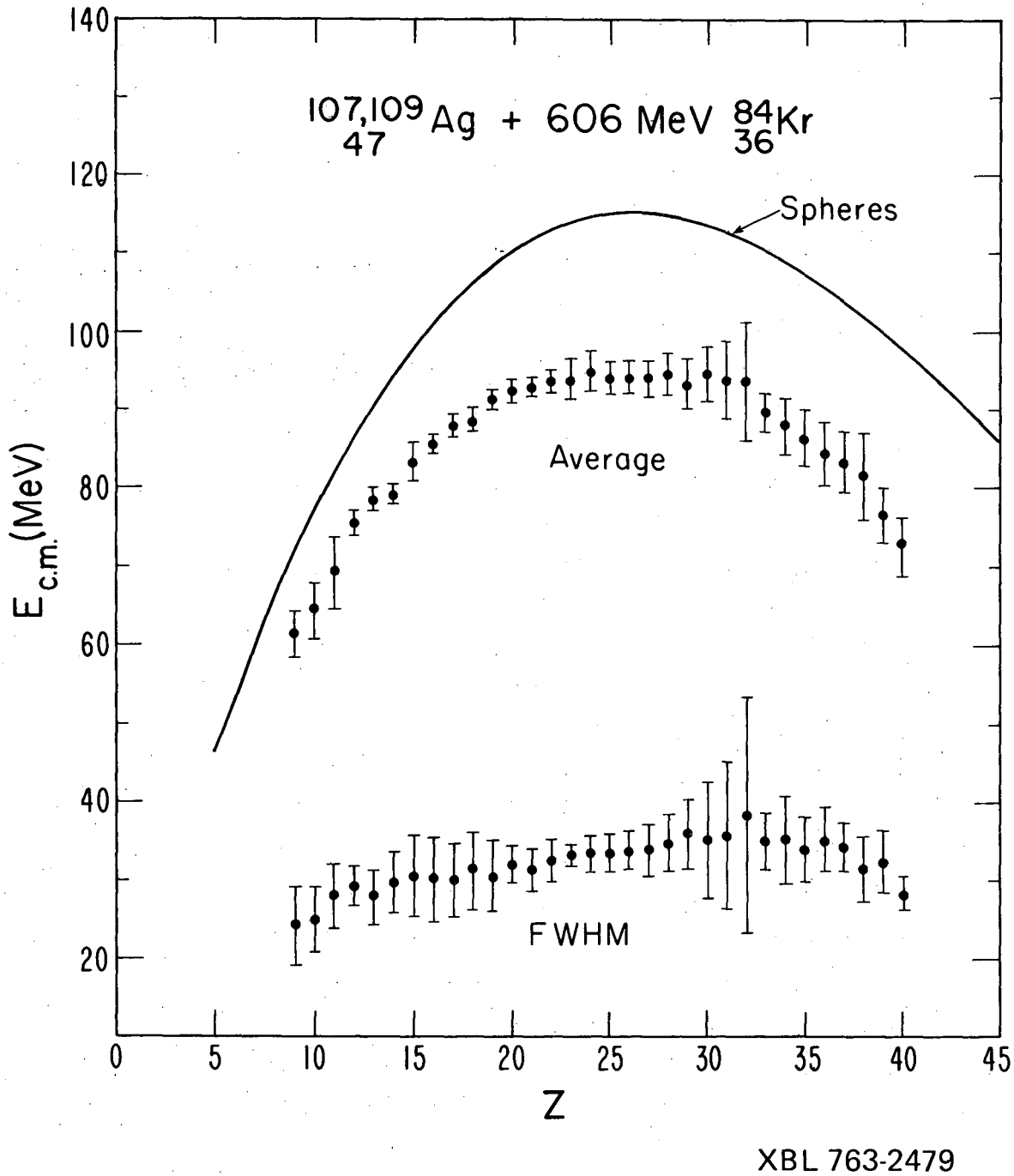
$^{107,109}_{47}$Ag + 606 MeV $^{84}_{36}$Kr
Spheres
Average
FWHM
$E_{c.m.}$(MeV)
Z
140
120
100
80
60
40
20
0
5
10
15
20
25
30
35
40
45
XBL 763-2479

Fig. 2

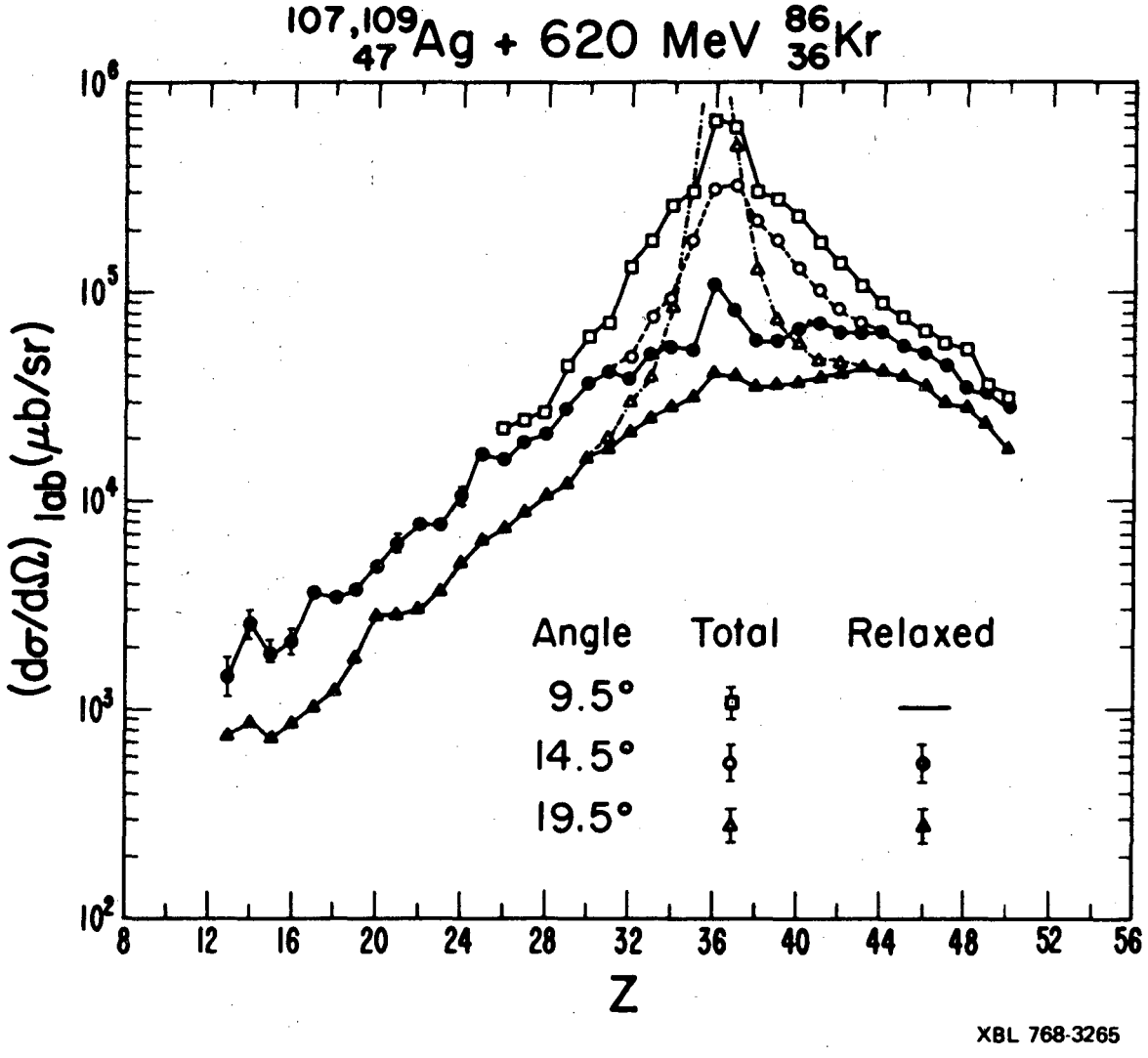

Fig. 3a

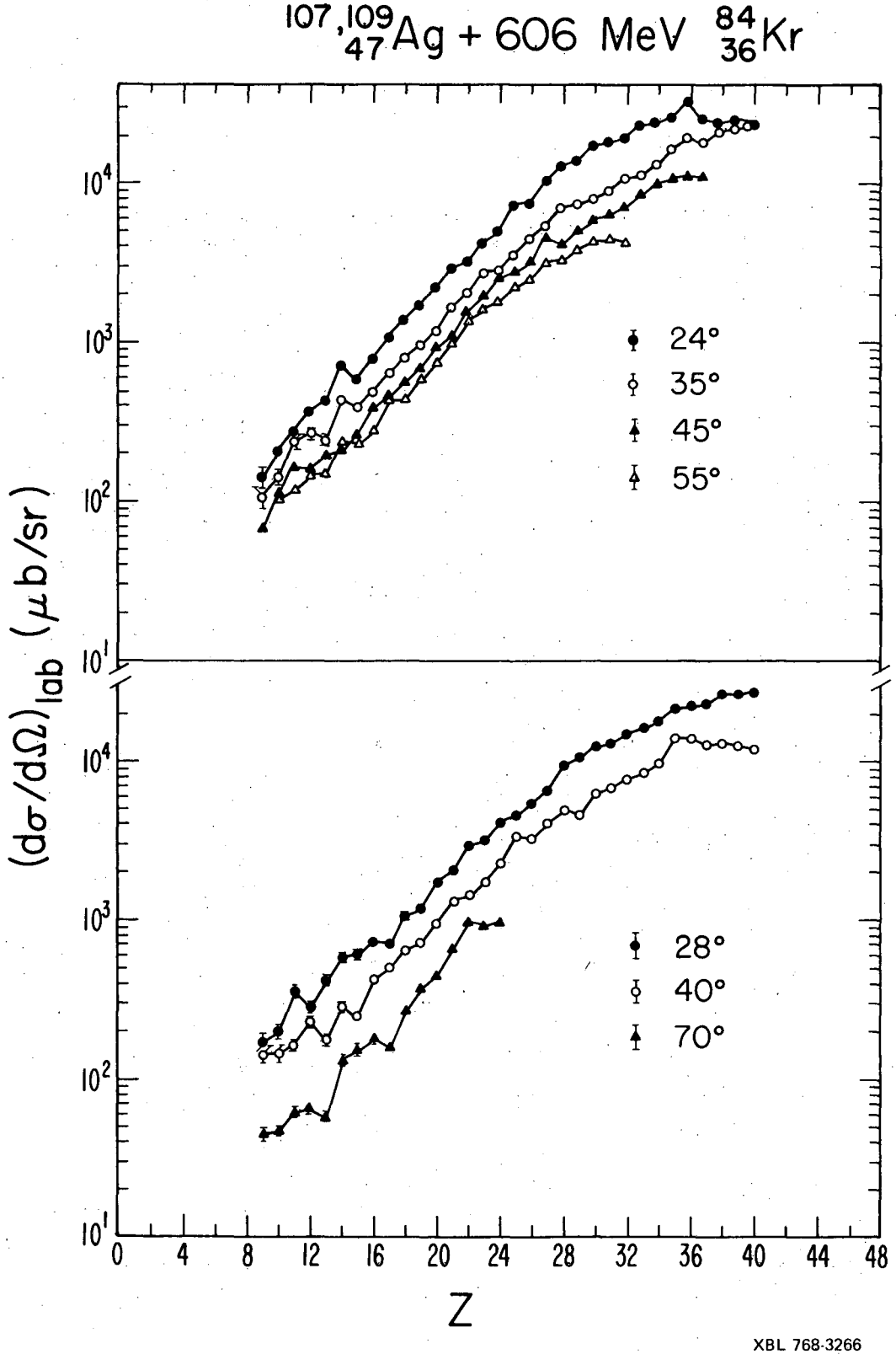
$^{107,109}_{47}$Ag + 606 MeV $^{84}_{36}$Kr
$(d\sigma/d\Omega)_{lab}$ (μb/sr)
24°
35°
45°
55°
28°
40°
70°
Z
XBL 768-3266

Fig. 3b

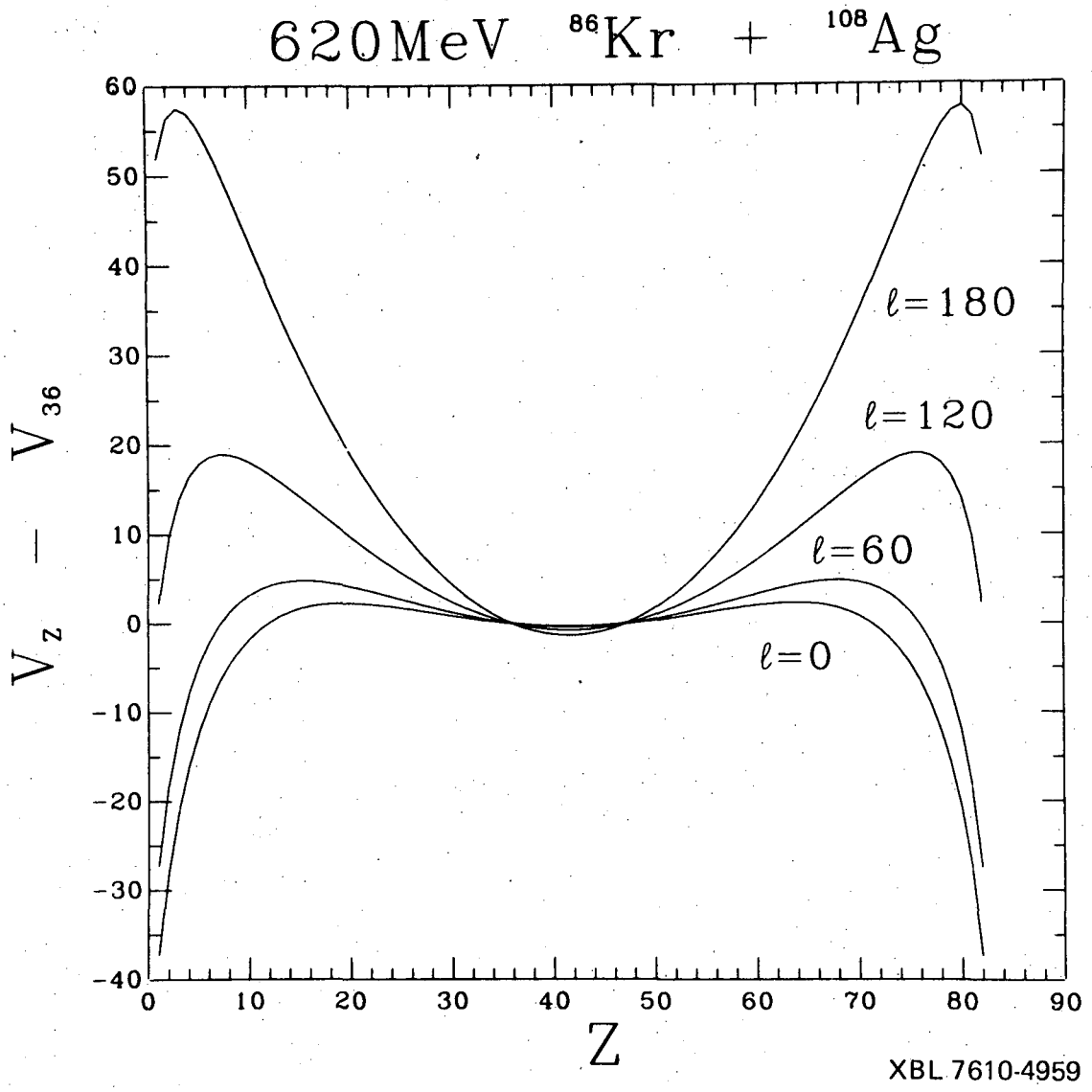

Fig. 4

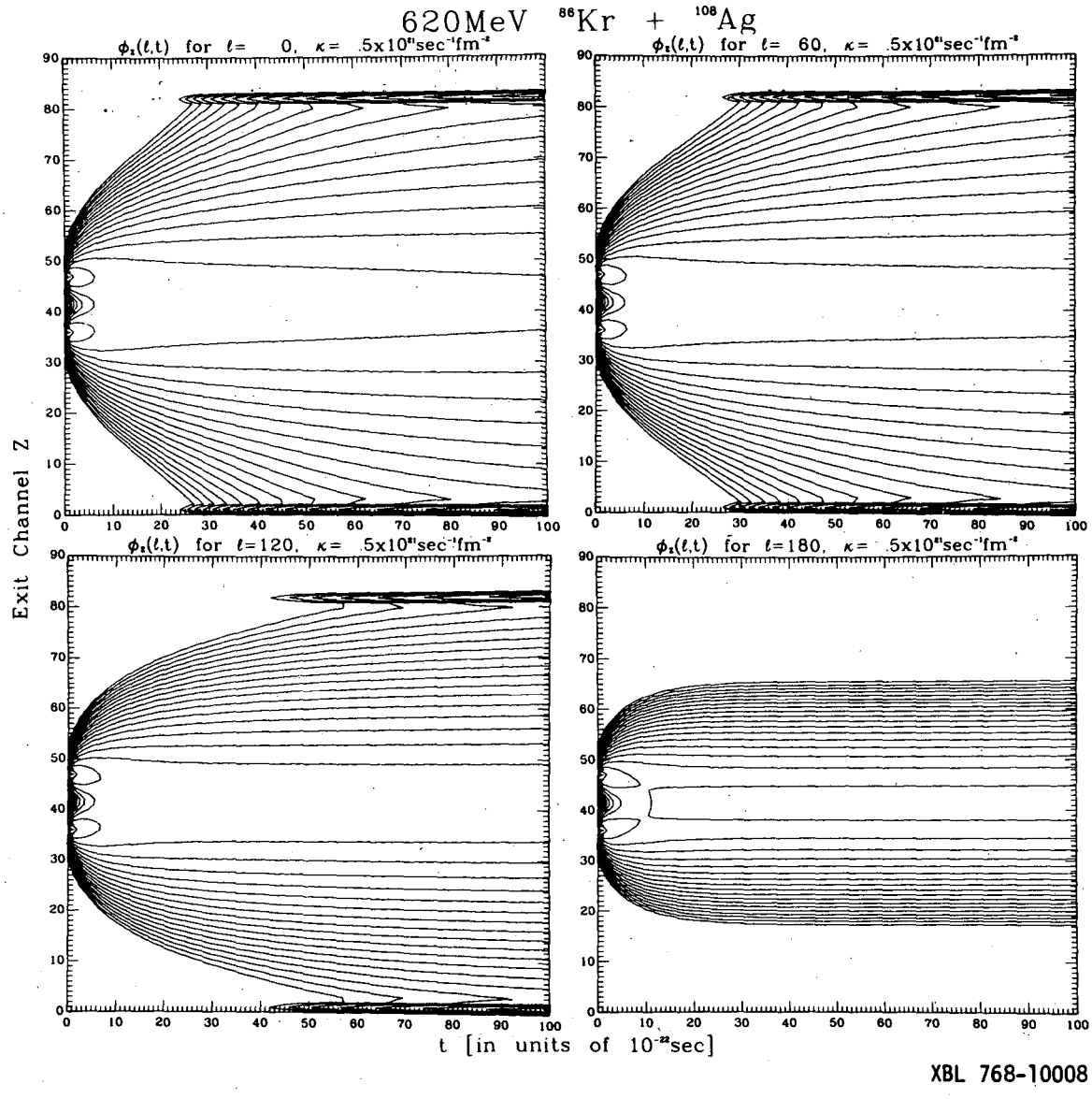
620MeV ^{86}Kr + ^{108}Ag
$\phi_z(\ell,t)$ for ℓ= 0, κ= .5x10^{41}sec^{-1}fm^{-2}
$\phi_z(\ell,t)$ for ℓ= 60, κ= .5x10^{41}sec^{-1}fm^{-2}
$\phi_z(\ell,t)$ for ℓ=120, κ= .5x10^{41}sec^{-1}fm^{-2}
$\phi_z(\ell,t)$ for ℓ=180, κ= .5x10^{41}sec^{-1}fm^{-2}
Exit Channel Z
t [in units of 10^{-22}sec]
XBL 768-10008

Fig. 5

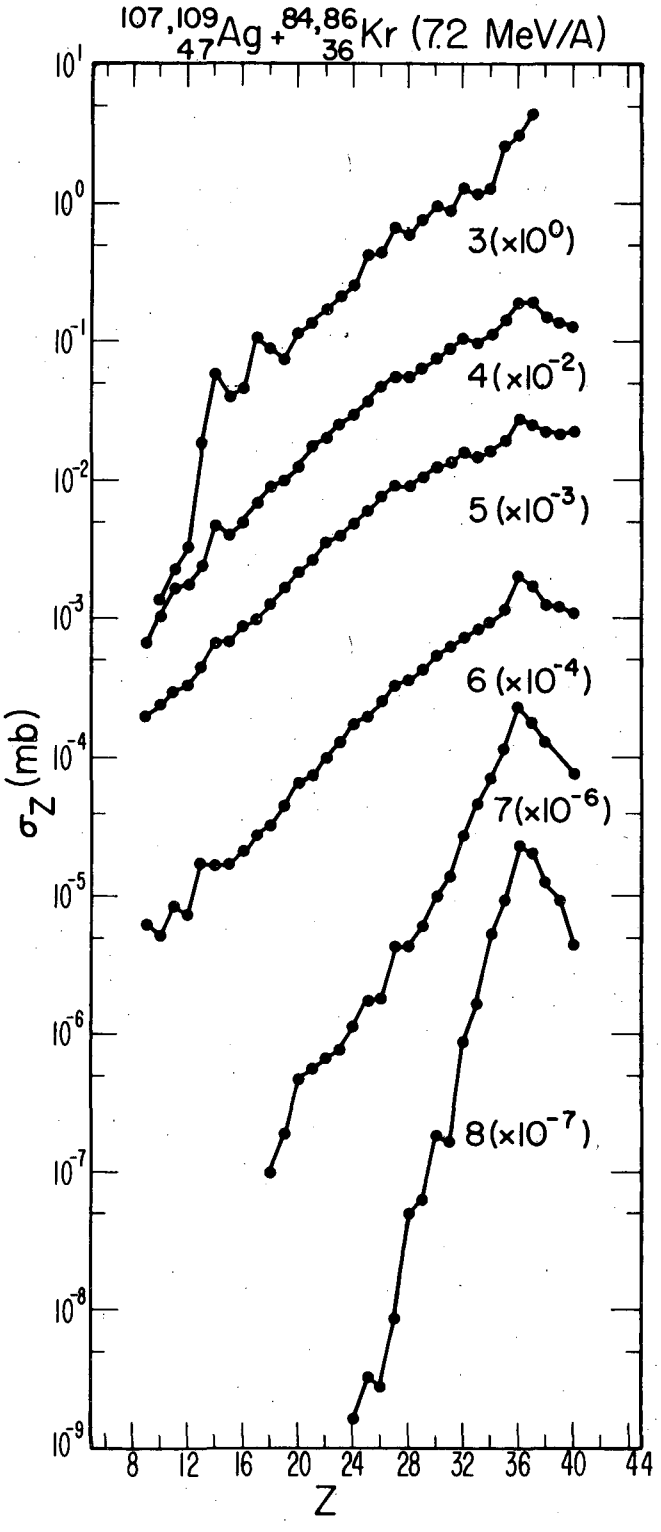
107,109 47Ag + 84,86 36Kr (7.2 MeV/A)
3(×10^0)
4(×10^-2)
5(×10^-3)
6(×10^-4)
7(×10^-6)
8(×10^-7)
σZ (mb)
Z
XBL 768-10147

Fig. 6

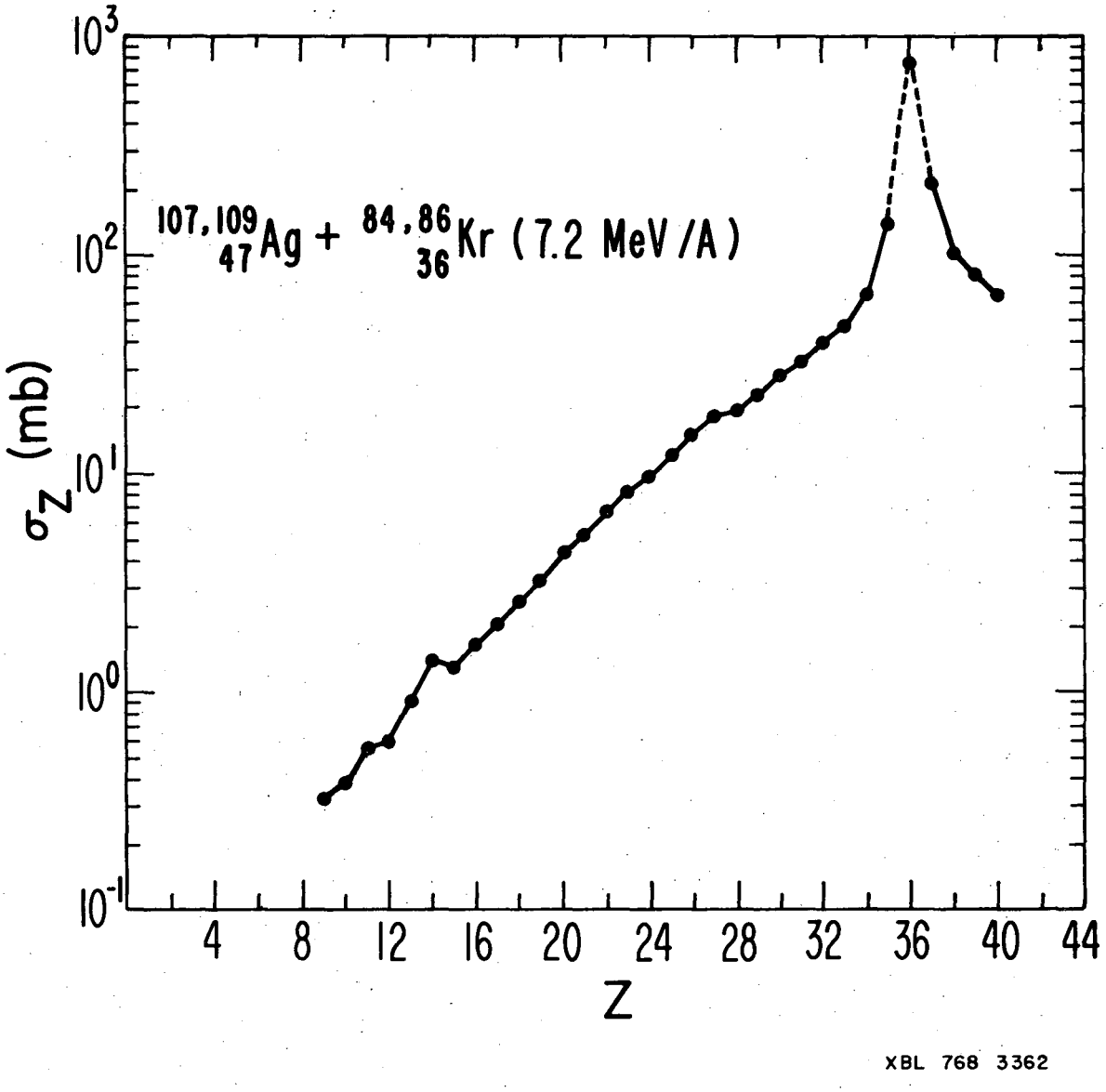
$^{107,109}_{47}Ag + ^{84,86}_{36}Kr$ (7.2 MeV/A)
σ_Z (mb)
Z
10^3
10^2
10^1
10^0
10^{-1}
4
8
12
16
20
24
28
32
36
40
44
XBL 768 3362

Fig. 7

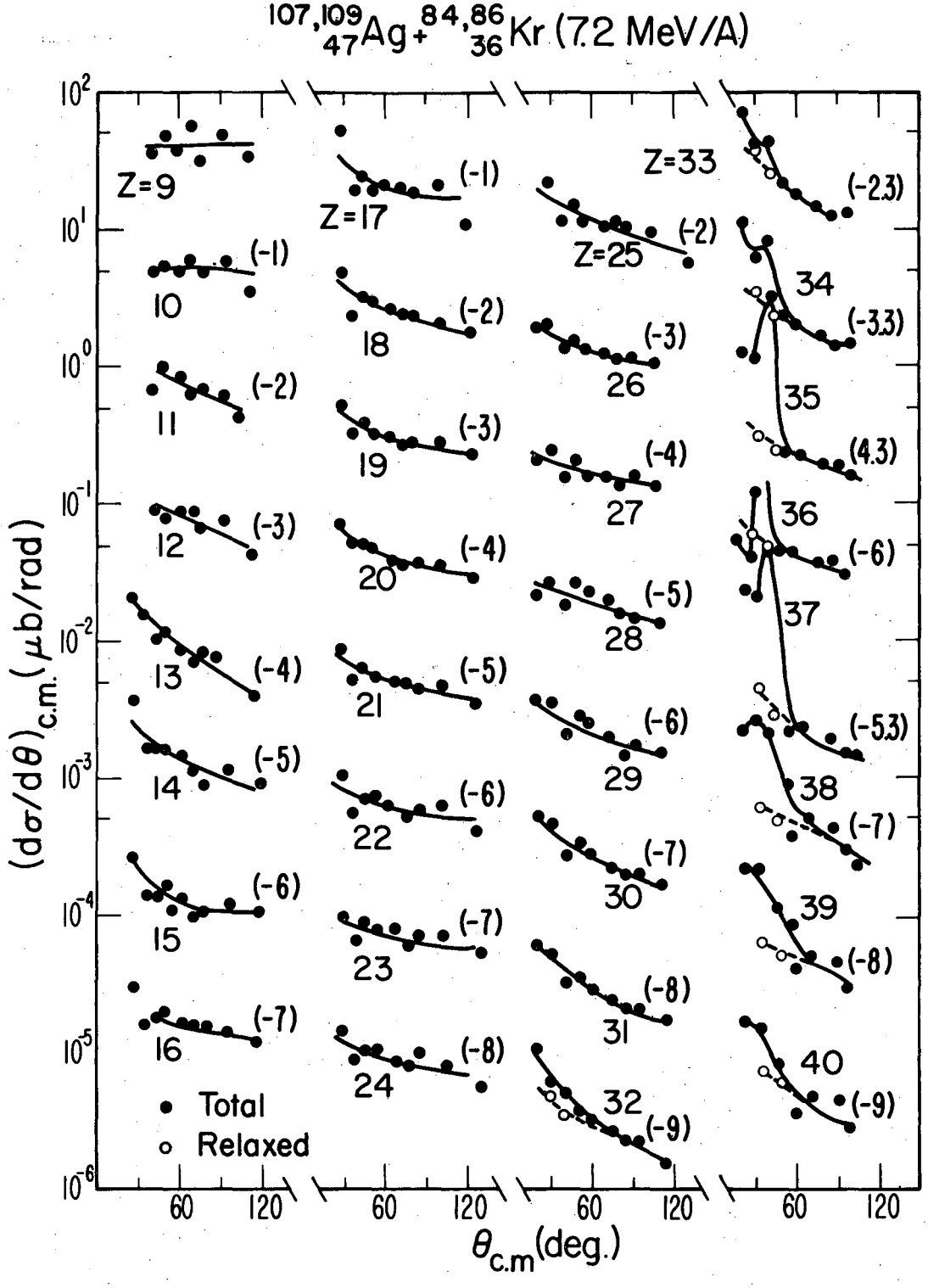

XBL 768-10148

Fig. 8

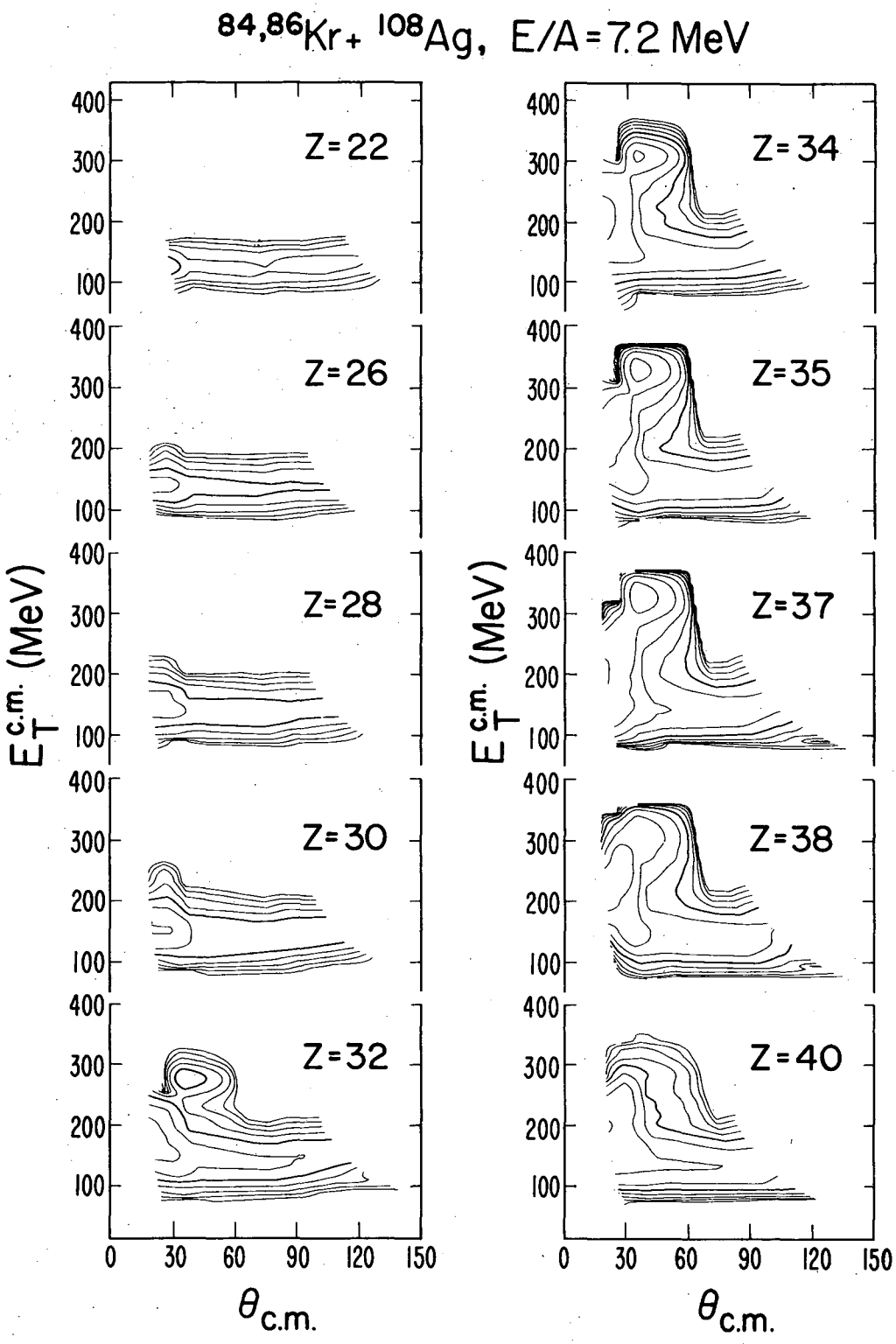

XBL 769 4076

Fig. 9

This report was done with support from the United States Energy Research and Development Administration. Any conclusions or opinions expressed in this report represent solely those of the author(s) and not necessarily those of The Regents of the University of California, the Lawrence Berkeley Laboratory or the United States Energy Research and Development Administration.

TECHNICAL INFORMATION DIVISION
LAWRENCE BERKELEY LABORATORY
UNIVERSITY OF CALIFORNIA
BERKELEY, CALIFORNIA 94720